energies

MDPI

Article

Comparison of Different Numerical Models for Solidification of Paraffin-Based PCMs and Evaluation of the Effect of Variable Mushy Zone Constant

Milad Tajik Jamalabad *, Cristobal Cortes, Javier Pallarés, Antonia Gil and Inmaculada Arauzo

Institute of Energy and Resources Efficiency of Aragón (ENERGAIA), University of Zaragoza, 50018 Zaragoza, Spain; tdyfqdb@unizar.es (C.C.); jpallare@unizar.es (J.P.); antgilma@unizar.es (A.G.); iarauzo@unizar.es (I.A.)

* Correspondence: mtajikjamalabad@unizar.es; Tel.: +34-695-675-007

Abstract: The impact of the mushy zone parameter (A_{mushy}) and the chosen numerical model during the solidification of a commercial paraffin-type phase change material (PCM) in a vertical cylinder under T-history conditions was examined through numerical simulations. The cooling process was modeled using three methods implemented in the CFD software ANSYS Fluent 2020 R2: the enthalpy–porosity method, the apparent heat capacity (AHC) method, and a new model proposed by the authors which incorporates heat capacity directly into ANSYS Fluent. To accurately define the boundary conditions, radiative heat transfer between surfaces was taken into account. Furthermore, the influence of the mushy zone parameter on the simulation accuracy and solidification rate was investigated, with the parameter being treated as a function of the liquid fraction. The results indicate that the proposed model aligns closely with experimental data regarding cooling temperature, offering better predictions compared to the other models. It was observed that temperature varies with time but not with position, suggesting that this model more effectively satisfies the lumped system condition—an essential characteristic of the T-history experiment—compared to the other methods. Additionally, the analysis showed that a higher mushy zone parameter enhances the accuracy of simulations and predicts a shorter solidification time; approximately 11% for the E-p and 7% for the AHC model. Using a variable mushy zone parameter based on the liquid fraction also produced similar results, resulting in an increased solidification rate.

Keywords: phase change material; variable mushy zone parameter; solidification; numerical simulation; paraffin-type PCM

check for updates

Citation: Tajik Jamalabad, M.; Cortes, C.; Pallarés, J.; Gil, A.; Arauzo, I. Comparison of Different Numerical Models for Solidification of Paraffin-Based PCMs and Evaluation of the Effect of Variable Mushy Zone Constant. *Energies* **2024**, *17*, 5982. https://doi.org/10.3390/en17235982

Academic Editor: Ioan Sarbu

Received: 8 November 2024
Revised: 20 November 2024
Accepted: 26 November 2024
Published: 28 November 2024

Copyright: © 2024 by the authors. Licensee MDPI, Basel, Switzerland. This article is an open access article distributed under the terms and conditions of the Creative Commons Attribution (CC BY) license (https://creativecommons.org/licenses/by/4.0/).

1. Introduction

Among renewable energy technologies, converting solar energy into thermal energy is currently one of the most widely adopted methods [1–4]. To maximize the efficient use of renewable energy in daily life and industrial applications, thermal energy storage technology is often necessary to stabilize energy output and ensure its effective utilization [5]. Phase change materials (PCMs) possess a robust capacity for energy storage and exhibit a noteworthy ability to maintain a consistent temperature while absorbing or releasing heat.

Numerous studies have investigated the solidification process of PCMs within a range of encapsulation geometries, including spheres, rectangular enclosures, and horizontal cylinders [6–12]. The melting and solidification behavior of a PCM with oscillations initiated at different times was investigated by Liu et al. [13]. They examined the effects of oscillation frequency and amplitude on melting performance and found that oscillation accelerates the phase transition process by enhancing convective heat transfer. Afaynou et al. [14] investigated the melting behavior of a PCM combined with metal foam and nanoparticles in a rectangular heat sink. The study examined the effects of various parameters, including porosity, nanoparticle concentration, and the type of metal foam.

Results indicated that a PCM/copper foam composite with high porosity and low PPI in the heat sink achieved a high heat transfer rate and a more uniform melting process. Additionally, using metal foam alone significantly improved the melting performance, while the inclusion of nanoparticles had a negative impact on the PCM's melting performance. Medjahed et al. [15] evaluated the thermal performance of a small-scale latent heat thermal energy storage (LHTES) model using beeswax as the PCM within a horizontally oriented shell-and-tube heat exchanger. Their findings showed that the discharging duration was significantly longer than the charging time, attributed to the gradual formation of a solid PCM layer around the exterior surface of the heat exchanger. Dardouri et al. [16] studied the effects of increasing the mass proportion of a paraffin and beeswax composite (PBPCM) within plaster. Key parameters—including density, thermal conductivity, specific heat capacity, thermal diffusivity, and latent heat—were experimentally analyzed. Results showed that increasing the PBPCM mass fraction in plaster reduced its thermal conductivity by more than threefold while enhancing heat retention, particularly by increasing the specific heat capacity. Zhao et al. [17] provided insights into promising thermal energy storage technologies for renewable energy applications aimed at achieving carbon neutrality. They first explored the relationship between renewable energy and thermal energy storage, followed by an introduction to the classifications of thermal energy storage systems and Carnot batteries. Reference [18] presents a systematic review of form-stable PCMs with recyclable skeletons, offering valuable insights for reducing carbon emissions and advancing sustainable energy development. The study examines the impact of recyclable skeletons on the thermophysical properties of form-stable PCMs. Kapilow et al. [19] conducted an experimental study on the melting and solidification of PCMs within a small-diameter vertical cylinder operating under convective boundary conditions. They employed air as the heat transfer fluid and studied the impacts of different air velocities and temperatures in their investigation. A three-dimensional model for evaluating various aspects of the discharge of a phase change material (PCM) enclosed within a vertical cylindrical enclosure was developed by Izgi and Arslan [20]. The computational model considers the influence of natural convection. Their findings show that natural convection plays a substantial role in the initial stages of the freezing process. Conduction subsequently becomes the dominant mechanism throughout the entire process. Furthermore, they reported that the diameter of the cavity significantly affects the freezing process, whereas changes in the cavity height do not have a noticeable effect.

Computational fluid dynamics (CFD) is an influential tool particularly adept at addressing complex, nonlinear problems involving the concurrent presence of mass, heat, and momentum transfer [21]. Consequently, it proves invaluable for simulating the thermal behavior of PCMs. The leading commercial CFD software packages include Ansys Fluent and COMSOL Multiphysics. Ye et al. [22] applied Ansys Fluent software 12 to research the fluid flow and heat transfer within a plate-fin unit. Ansys Fluent's solidification and melting model is based on the enthalpy–porosity method, which is a widely employed tool for investigating phase change phenomena. Nowadays, substantial research efforts have been dedicated to utilizing this model, yielding valuable agreements with experimental findings [23–26].

Numerical phase change models in the literature are generally categorized into two main groups: fixed-grid (or continuum) models and variable-grid (or two-phase) models [27]. Fixed-grid models apply a single computational domain where continuity, energy conservation, and momentum equations are used uniformly across the entire domain. In contrast, variable-grid models use separate computational domains for the solid and liquid phases, coupled through transfer terms between the phases [28]. As a result, fixed-grid models are simpler to implement than variable-grid models, while still providing accurate results [29]. Nazzi Ehms et al. [30] provide a clear classification of fixed-grid models for the solidification and melting of PCM, organized by latent heat modeling and velocity transition modeling. Latent heat models, applied within the energy equation, can be based on a source term, enthalpy, or temperature. Temperature-based models are further

categorized into three types: apparent heat capacity, effective heat capacity, and heat integration. Additionally, velocity transition models are classified into three main groups: the switch-off method, the source term method, and the variable viscosity method. Moreover, Li et al. [31] present axisymmetric, enthalpy-based Lattice Boltzmann models for simulating solid–liquid phase changes. Their findings indicate that these models effectively simulate axisymmetric solid–liquid phase transitions.

The numerical simulation of a PCM requires inputting material properties and parameters as input values. The mushy zone is where the melting or solidification process starts and progresses, during which latent heat is absorbed or released. Therefore, an accurate representation of the solid–liquid phase change and the associated latent heat storage performance is crucial. This parameter is part of a source term in the Carman–Kozeny equation, which is used in the enthalpy–porosity technique for the momentum equation to simulate the flow resistance through the mushy zone. This approach addresses the main drawback of the fixed-grid method, which struggles with handling the zero-velocity condition as the liquid transitions to a solid within the mushy zone. The main questions are how the mushy zone constant A_{mushy} affects the predicted solidification performance and how to determine A_{mushy}. While the Carman–Kozeny equation is commonly used in most models, the effects of the A_{mushy} parameter continue to be a topic of frequent investigation [32]. Values for A_{mushy} ranging from 10^3 to 10^{10} have been recommended in commercial software guidelines and by various researchers [33]. The melting of lauric acid was numerically studied by Abdi et al. [34] and they proposed an A_{mushy} value of 10^6 kg/$\left(\mathrm{m}^3\cdot\mathrm{s}\right)$ because it was closer alignment with experimental data than the values of 10^5 and 10^7 kg/$\left(\mathrm{m}^3\cdot\mathrm{s}\right)$. Similar research has been conducted by Hong et al. [35]. Fadl et al. [36] reported that the optimal A_{mushy} values are 5×10^5 and 2×10^5 for the vertical and horizontal orientations, respectively. The most common value for A_{mushy} is the recommended 10^5 kg/$\left(\mathrm{m}^3\cdot\mathrm{s}\right)$ [37–40]. Kheirabadi et al. [33] suggested that for lauric acid, the optimal value for A_{mushy} is 10^6 when ANSYS FLUENT and COMSOL Multiphysics solvers are used. A_{mushy} significantly impacts the accuracy and correctness of the predicted melting performance. However, its role in predicting solidification performance remains poorly reported to date. It is quite interesting to examine how this flow resistance parameter affects solidification and to understand the extent of its influence on the related heat recovery performance.

This research aims to investigate the impact of the numerical model and the mushy zone parameter on phase change solidification simulations, using paraffin as a representative phase change material. The cooling process was simulated using three methods implemented in the CFD code ANSYS Fluent 2020 R2 [41]: the enthalpy–porosity method, the AHC method, and a new model proposed by the authors in which heat capacity is directly introduced into ANSYS Fluent. Furthermore, the impact of the A_{mushy} on the accuracy and correctness of the predicted solidification performance has been investigated by testing different values of A_{mushy} (constant and variable). The results, such as temperature profiles, solidification time, and solidification profiles, are analyzed scientifically. This paper offers a detailed discussion of the observed differences and how they change with varying model parameters, providing explanations in physical terms. This research aims to provide a more accurate approach to studying the effects of simulation methods and the mushy zone constant on the solidification process in a vertical cylinder under real boundary conditions.

2. Methodology

2.1. Physical Model

The physical model in this study is based on the authors' experimental work, which examined the solidification of paraffin-based PCMs under T-history conditions [42,43]. The schematic diagram of the 2-D simulation geometry is presented in Figure 1. A rectangular computational domain was defined, taking into account two distinct fluid regions: one containing air and the other comprising the working substance, either water or a PCM.

The tube has a diameter of 30 mm and a height of 170 mm, with 140 mm filled with a liquid PCM. In the upper part, a rubber plug was modeled via a thin-wall thickness approach, incorporating combined heat transfer around it. Moreover, the model was numerically simulated, assuming axisymmetric conditions, incompressible laminar flow, and the Boussinesq approximation for buoyancy effects. For solidification, the external wall was designed to account for heat losses via conduction, convection, and radiation to the surrounding environment, as depicted in the equivalent thermal circuit in Figure 1. To calculate surface emissivity and radiation heat transfer, the authors [42] proposed a numerical method that reduces computational costs and simulation time, improving the efficiency of thermal analysis while maintaining accuracy.

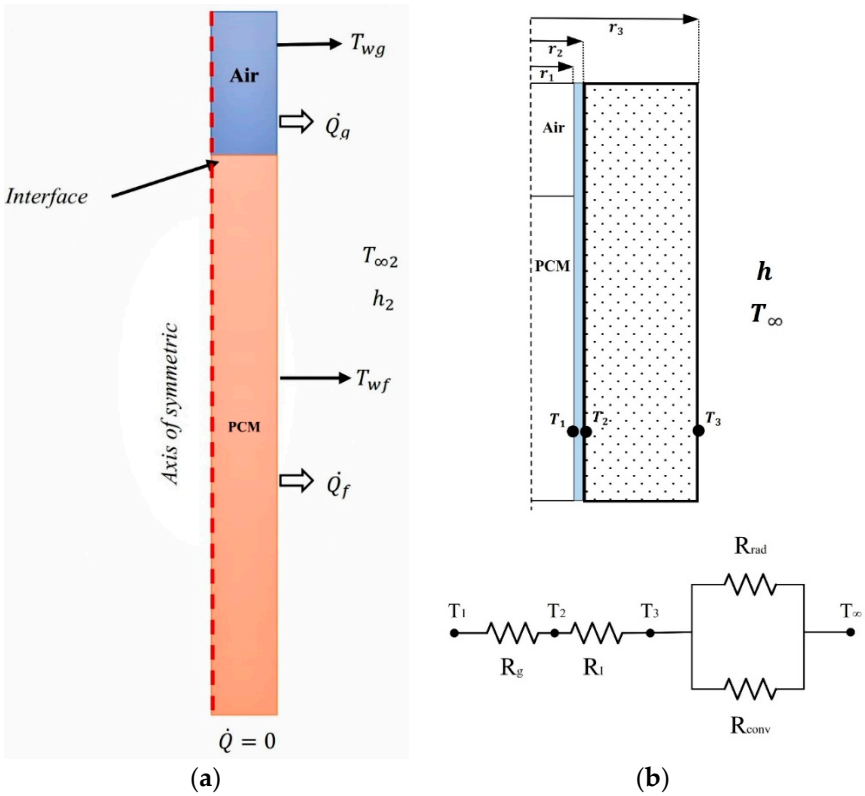

Figure 1. (**a**) The scheme of the computational model and (**b**) equivalent thermal resistance.

2.2. Governing Equations

2.2.1. Enthalpy–Porosity Method

The enthalpy–porosity technique has been extensively applied in simulating the melting and solidification phenomena within PCM enclosures, particularly when natural convection plays a significant role. When dealing with fusion and solidification within a fixed domain, adjustments to the momentum equation are necessary to accommodate phase transitions, ensuring zero velocities in the solid phase. A common approach to address this involves incorporating a high-magnitude source term (S_u) into the momentum equation.

$$\frac{\partial}{\partial t}(\rho u_i) + \frac{\partial}{\partial X_j}(\rho u_i u_j) = -\frac{\partial p}{\partial X_i} + \mu \frac{\partial^2 u_i}{\partial X_j \partial X_j} + \rho g_i + S_u \quad (1)$$

where ρ is the density and where μ is the dynamic viscosity. The term S_u modifies the moment balance depending on the phase. The term varies, ranging from a high value that enforces complete immobility in the solid region to eventually reaching a limit of zero as the material transitions into a fully liquid state. The source term of Equation (1) is defined as

$$S_u = -A(\gamma)u_i \quad (2)$$

here, A (γ) is the porosity function, which allows the moment equation to mimic the behavior of the flow in the mushy region of the PCM, defined by the Carman–Kozeny equation derived from Darcy's law for a porous medium [44]:

$$A(\gamma) = \frac{A_{mushy}(1-\gamma)^2}{\gamma^3 + \varepsilon} \tag{3}$$

where γ is the liquid volume fraction and where A_{mushy} is the constant of the mushy zone, which varies according to its morphology. Higher values of A_{mushy} result in stronger velocity damping, leading to a thinner mushy region and approaching a situation resembling that of a pure substance. The constant ε is introduced to prevent division by zero.

Voller [44] initially introduced the enthalpy–porosity technique to address phase change problems related to convective diffusion-controlled heat transfer. The energy equation can be written as

$$\frac{\partial \rho H}{\partial t} + \vec{\nabla}\cdot(\rho \vec{\vartheta} H) = \vec{\nabla}\cdot(\lambda \vec{\nabla} T) \tag{4}$$

The governing energy equation thereby contains one enthalpy H that includes latent and specific heat:

$$H(T) = \int_{T_m}^{T} C_p dT + \rho\gamma L \tag{5}$$

where ρ corresponds to the density, C_p corresponds to the specific heat and L corresponds to the latent heat of the PCM. L is associated with the liquid fraction, γ, which allows the computation of the change in enthalpy from the energy in the material during the phase change [43]. The general form of γ can be written as

$$\gamma = \begin{cases} 0 & if\ T < T_s \\ \frac{T-T_s}{T_l-T_s} & if\ T_s < T < T_l \\ 1 & if\ T > T_l \end{cases} \tag{6}$$

In this formulation, the porosity is equated to the liquid fraction, f_l, within a given element, as dictated by the enthalpy balance. The liquidfraction is recalculated for each iteration. The "mushy zone" refers to the region where the liquid fraction ranges from 0 to 1. Consequently, when a material is completely solidified within an element, the porosity decreases to zero. During the phase change from liquid to solid, the velocity decreases to zero, making it crucial to accurately incorporate this phenomenon in the numerical formulation. Researchers have employed various methods [45] to implement this aspect of physics.

2.2.2. Apparent Heat Capacity (AHC)

The apparent heat capacity (AHC) method takes into account the influence of enthalpy and its temporal evolution by incorporating an apparent heat capacity during thermal phase transitions. The approach is based on the following relationship:

$$\frac{\partial H}{\partial t} = \frac{\partial H}{\partial T}\frac{\partial T}{\partial t} \tag{7}$$

where $\frac{\partial H}{\partial T} = \rho c_{app}(T)$ represents the temperature-dependent apparent heat capacity. The apparent specific heat capacity is calculated as the derivative of the specific enthalpy, taking into account a temperature-dependent phase change enthalpy [45].

$$c_{app}(T) = (1-\gamma)c_p^s + \gamma c_p^l + \frac{d\gamma}{dT}(h^l(T) - h^s(T)) \tag{8}$$

where $h^s(T)$ and $h^l(T)$ represent the extrapolated single-phase specific enthalpies for the solid and liquid states, respectively [46].

In the enthalpy porosity model, $\gamma(T)$ represents a linearly increasing liquid fraction between the solidus and liquidus temperatures, assuming constant values (zero and one) outside the phase change temperature range. Buruzs et al. [47] indicate that the non-differentiable nature of this piecewise linear liquid fraction function can lead to convergence problems, so they introduced an alternative relation for $\gamma(T)$ based on the smooth step function and cubic Hermite spline functions [46].

2.2.3. New Model

In the proposed model, the heat capacity of the PCM is determined through Differential Scanning Calorimetry (DSC) and implemented in ANSYS FLUENT software using a User-Defined Function (UDF) file. It is important to note that DSC results are highly sensitive to varying heating and cooling rates; therefore, heat capacity is calculated at heating rates of 1, 5, 10, and 20 °C/min. The methodology is simple: the obtained specific heat capacity curve as a function of temperature ($c_p - T$) from DSC is used as a variable, the specific heat capacity of the material, in ANSYS FLUENT software 2020 R2. One of the primary heat transfer phenomena in phase change is natural convection, which arises from temperature-induced density differences. Without accounting for variable density, the model reduces to a conduction problem, addressing only pure diffusion and neglecting the movement within the liquid phase. Since convection is incorporated in the enthalpy–porosity model, and it is likely to be important in our problem, we use the following generalization [48,49]. The technique of a source term S_u in the momentum equation will relate linearly the enthalpy with the liquid fraction and thus lead to numerical results similar to those of the enthalpy–porosity method. Instead, we model a liquid with a viscosity that varies with temperature according to our measurements on the liquid PCM above the solidus point, and below we fair a temperature function reaching a significantly high value. This assures that velocity of the medium decreases in the mushy region and finally stops when it is a solid.

$$\mu_l = \begin{cases} -\left(2.273 \times 10^{-1}\right) T + 33.83 & T \leq T_s \\ \left(2.283 \times 10^{-7}\right) T^3 - \left(3.501 \times 10^{-5}\right) T^2 + \left(1.73 \times 10^{-3}\right) T - 0.02587 & T > T_s \end{cases} \quad (9)$$

An overview of the differences between the three models is presented, highlighting how each incorporates heat capacity and determines the flow resistance of the liquid phase. A summary of these models is outlined in the Table 1 below.

Table 1. Comparison of the three numerical methods.

Numerical Method	Heat Capacity	Flow Resistance
enthalpy–porosity	constant value	source term, Equation (2)
AHC	apparent specific heat capacity, Equation (8)	source term, Equation (2)
new model	specific heat capacity as a function of temperature from DSC	variable viscosity, Equation (9)

2.3. Numerical Model Setup

The numerical model setup parameters were chosen on the basis of ANSYS FLUENT guidelines [41] and previous research papers [27,30,40,42] that have numerically studied the phase change process.

The ANSYS Fluent 2022 R2 code was employed to simulate the solidification process. The conservation equations for both momentum and mass were addressed via the semi-implicit method for the pressure-linked equations (SIMPLE) algorithm. The momentum and energy equations were discretized via a second-order upwind scheme and pressure correction was carried out via the PRESTO! (PRESure STaggering Option) method. Relaxation factors of 0.3, 0.7, and 1 were applied to pressure, momentum, and energy, respectively. At

each time step, the convergence of the solution was verified throughout the simulation. These modeling choices align with the recommendations in [40,42].

2.4. Mesh Tests

To confirm that the results are independent of the chosen mesh (grid) resolution, various element sizes were tested and compared with experimental results over the entire process duration. Structured meshes with 65,844, 23,800, 6120, and 2332 quadrilateral elements were employed. Parameters such as the maximum aspect ratio, orthogonality, cell quality, and obliquity were meticulously adjusted to meet the recommended criteria. In Figure 2, a close alignment is observed between the experimental findings and the numerical model when water is used as the working fluid. There are no substantial disparities in the simulated cooling curves across various mesh sizes compared with the experimental results.

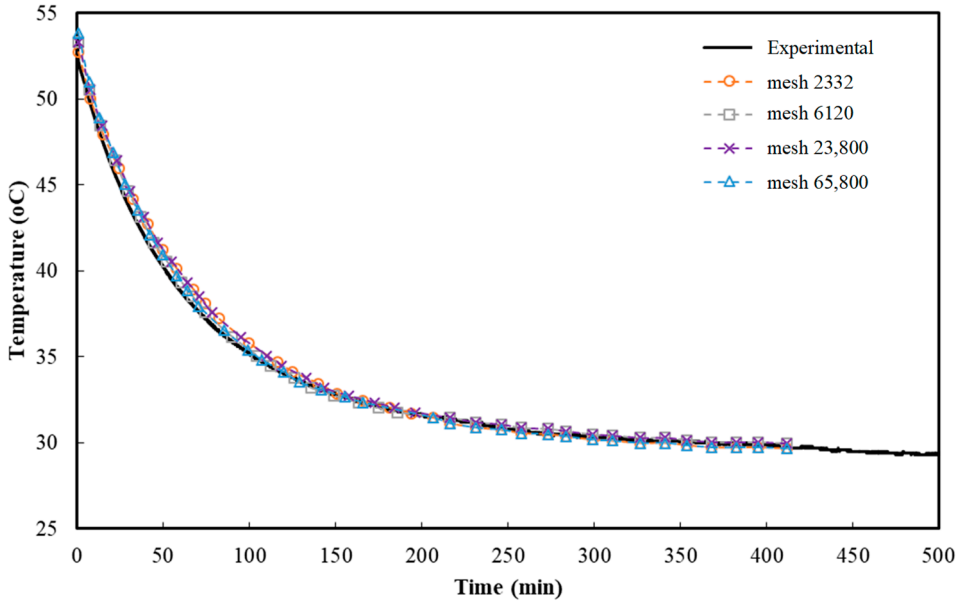

Figure 2. Results of independent of the chosen mesh for simulation with water.

3. Numerical Results

In this section, numerical results are presented to examine the influence of the thermal properties of the PCM and the mushy zone parameters on the solidification process. The numerical modeling was conducted under the assumptions that (1) the flow is laminar and incompressible, (2) the material properties in each simulation remain constant, as indicated in Table 1, (3) the Boussinesq approximation was applied, and (4) the domain is modeled as a fluid in which the solid phase has a high viscosity.

Figure 3 illustrates the PCM cooling process employing the enthalpy–porosity method with a mushy zone constant (C) value of 105. The PCM properties were inputted based on the manufacturer's provided values, as detailed in Table 1. The Boussinesq approximation was used for buoyancy due to variable density. The graph reveals two noteworthy observations. First, the numerical cooling curves exhibited a consistent pattern across the various mesh sizes, with no notable discrepancies. Second, there is a noticeable abrupt shift in the cooling curve at the start and end points of solidification (at 46 and 40 °C, respectively) in the numerical simulation. In contrast, under real experimental conditions, a much more gradual change in slope is observed, especially at the end.

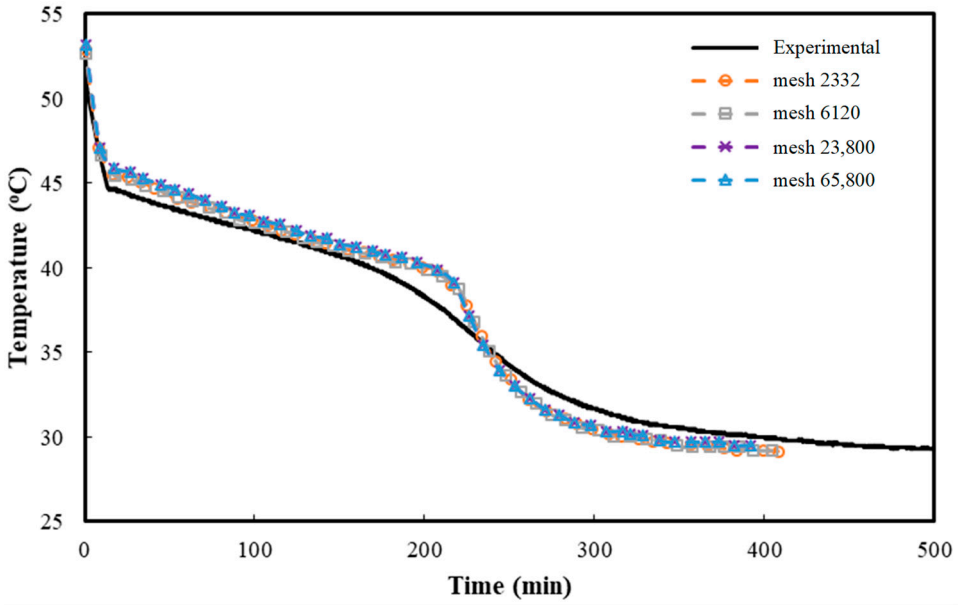

Figure 3. PCM simulation results using the enthalpy method.

This study is divided into two main sections. The first part focuses on investigating the influence of the numerical model on phase change solidification simulation using paraffin as a sample phase change material to determine which model is more accurate. The second part examines the effect of the mushy zone parameter on solidification, comparing constant and variable mushy zone parameters to identify the optimal values for use in numerical modeling of the phase change process for paraffin material.

3.1. Comparing the Three Numerical Methods

As outlined in Section 2.2, three different numerical models were used to simulate the solidification of PCM-paraffin under T-history conditions. Figure 4 shows the temperature during the solidification process for all models. The new model aligns most closely with the experimental data compared to the others, while the E-p and AHC models exhibit a slight discrepancy with the experimental results. Specifically, for the E-p model, there is a noticeable abrupt shift in the cooling curve at the start and end points of solidification (at 46 and 40 °C, respectively). In contrast, under real experimental conditions, a much more gradual change in slope is observed, especially at the end. Although the AHC model has a good agreement with the experimental result, the new model demonstrates a more precise change in the solidification slope, which aligns more closely with the experimental results. To compare the results obtained concerning the experimental data, the mean absolute percentage error (MAPE), which is also known as the mean absolute percentage deviation (MAPD), was used. The variations in the cooling curves of the new model and AHC model compared with the experimental curve showed percentage errors (EPAM) of 3.1% and 8.3%, respectively. Reference [47] reported similar results, demonstrating that using the ACH method improves simulation accuracy compared to the enthalpy–porosity method.

Figure 5 presents the comparison of the liquid fraction for the three models. Although the liquid fractions for all models are similar at the beginning of the solidification process, a noticeable discrepancy between them emerges towards the end of solidification. Moreover, the solidification profile of the new model differs significantly from the others. Initially, the solidification rate of the new model is faster than the other models, but it slows down as the process progresses, ultimately resulting in a slightly shorter total solidification time compared to the other two models. Moreover, the new model shows a change in the gradient of the liquid fraction, with a distinct maximum point for the solidification rate. In other words, the new model shows that the solidification rate initially rises sharply to a peak, then decreases through the middle of the process. Following this, a gradual increase

occurs until a local maximum is reached, after which the rate declines to zero. The same pattern has been observed for AHC but not for the E-p model (Figure 5b). This phenomenon has been noted by Milad et al. [43], who also showed that the solidification rate reaches a maximum point during the process. Furthermore, an examination of the slope of the liquid fraction curve revealed that the rate of solid formation initially increased, peaked, and then steadily decreased to zero as the solidification process progressed. Reference [50] explained that this phenomenon occurs because, initially, numerous nuclei form and the crystals grow larger due to liquid subcooling. This causes an enhancement in the solid formation rate. However, as solidification progresses, continuous nucleation events are effectively inhibited. This suppression occurs because the thermal gradient driving the phase change decreases as the nucleation site moves farther from the cooling wall and the thermal resistance rises. As a result, the entire solidification process gradually slows.

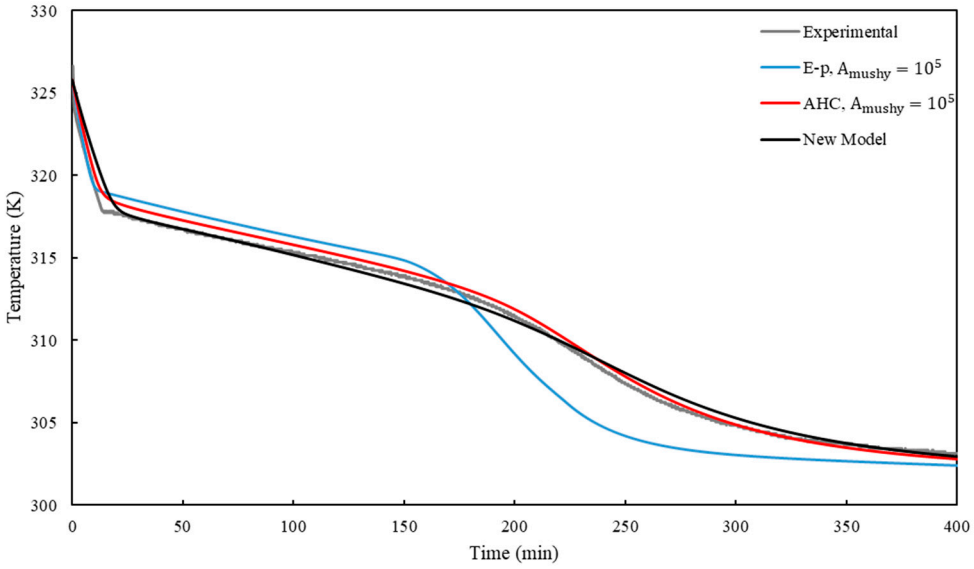

Figure 4. Comparison of cooling curves for different three numerical models.

The key characteristic of the T-history experiment is that the Biot number satisfies the lumped system analysis condition (Bi < 0.1). This implies that the temperature varies with time but not with position, meaning the temperature of the medium changes uniformly over time.

Figure 6 illustrates the temperature difference between the centerline and the wall for the three points (Y = 3.5, 7, and 10.5 cm). The new model demonstrates a minimal temperature difference, fluctuating between 1.25 and 0.5 K. A similar pattern is observed in the AHC model, where the temperature difference remains within a narrow range. In contrast, the E-p model causes more uneven temperature changes, with discrepancies ranging from 2.0 to 0.4 K. Another interesting observation is that, although a slight variation is seen in the E-p model when moving from the bottom to the top of the tube, both the AHC model and the new model show an almost unchanged temperature pattern along the tube's length. In fact, with these two models, the temperature difference between the centerline and the wall remains consistent, regardless of the measurement point's location. Moreover, during the solidification process, the cooling rate of the PCM decreases, likely due to the release of latent heat, increased thermal resistance from the growing solid phase, or a combination of both factors, as the temperature of the sample and ambient environment approach each other. This indicates that the Biot number decreases during solidification, resulting in a smaller temperature difference between the centerline and the wall of the tube. The new model clearly illustrates this phenomenon.

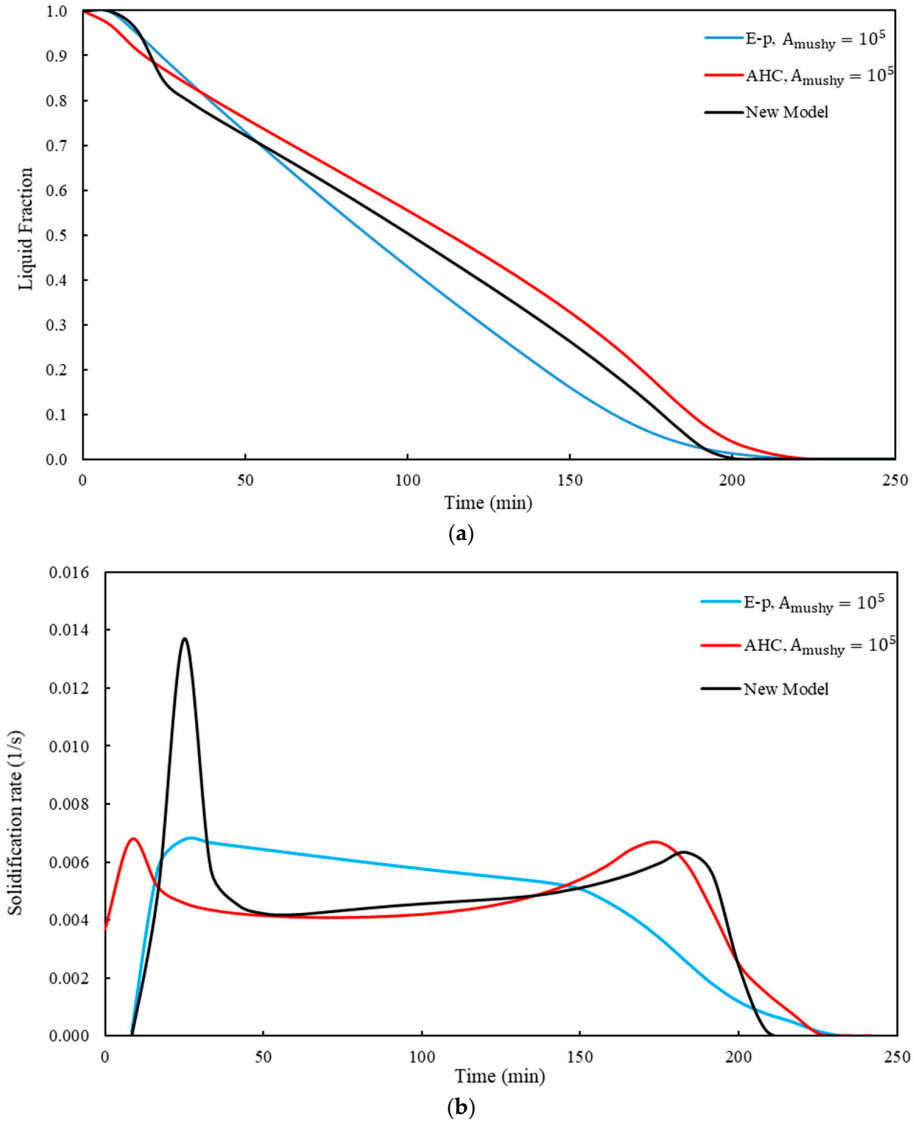

Figure 5. (**a**) Liquid fraction of solidification process and (**b**) solidification rate.

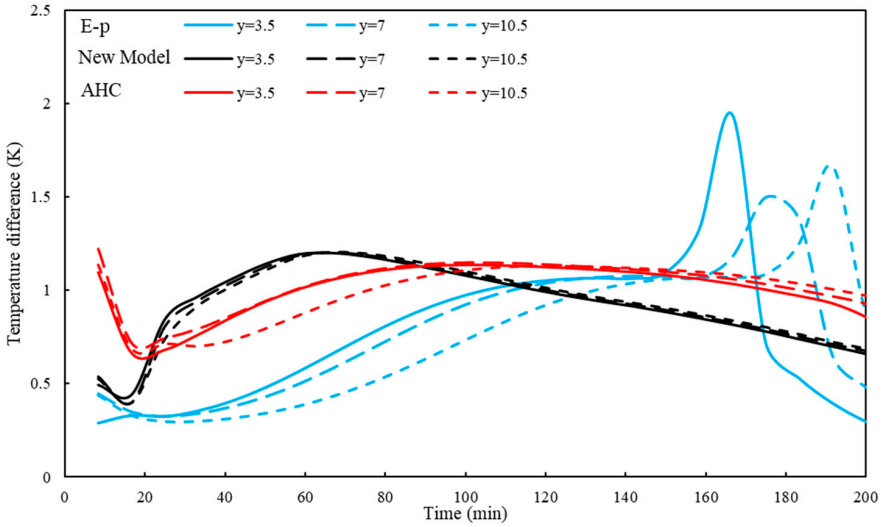

Figure 6. Temperature difference between the centerline and the wall for the three points (Y = 3.5, 7, and 10.5 cm).

Figure 7 compares the solidification profiles for three models over a 150–200 min period. The primary observation is that the solidification profiles differ based on the simulation model. As anticipated, the solidification rate in the E-p model is lower than in the other models during this timeframe. After 150 min, solidification begins to progress at the bottom of the tube in the E-p model, a pattern not observed in the other two models. Although solidification develops at the tube's bottom in both the E-p and ACH models, in the new model, it slows in the bottom layers and instead concentrates near the cold wall. This discrepancy in the solidification profile behavior is directly related to the heat transfer characteristics in the mushy region.

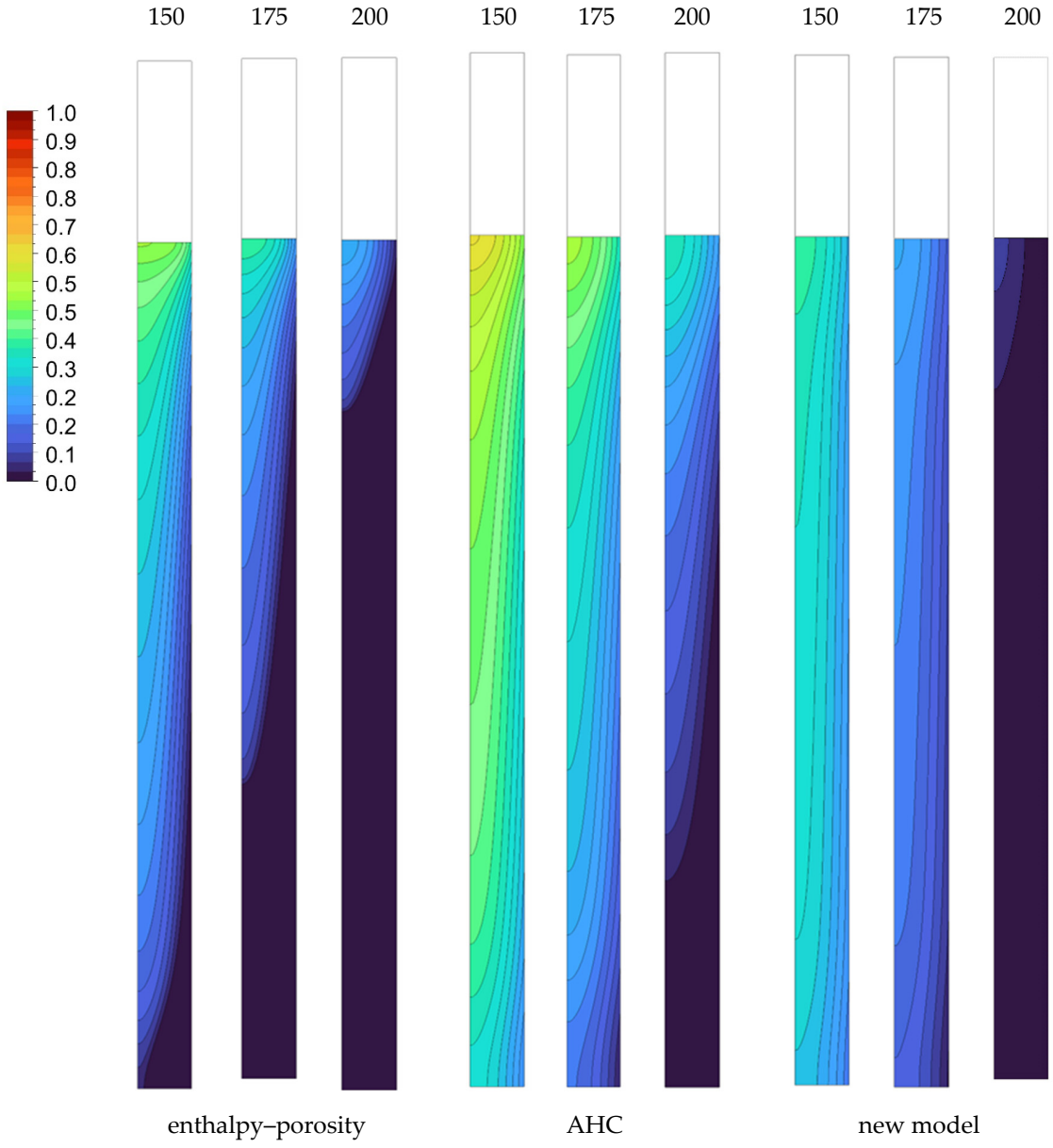

Figure 7. Comparison of the solidification profile for three models.

3.2. The Effect of the Mushy Zone

In order to examine the impact of the mushy zone parameter, several simulations for different mushy zone parameters of 10^5–10^8 were conducted. Liquid fractions throughout the solidification process were investigated for each set of simulations, as they are directly influenced by the mushy zone parameter.

Numerous studies suggest a reliable method, grounded in the physical characteristics of the mushy zone, to determine the mushy zone constant, A_{mush}. For various PCMs, the A_{mushy} value can be determined as a function of dynamic viscosity and the characteristic length of solid microstructures within the mushy zone. A_{mushy} is a parameter that relates the microstructural characteristics of the mushy zone to macroscopic heat transfer during phase change. Yang et al. [51] evaluated the A_{mush} parameter based on measured microstructural features and proposed the A_{mushy} value function of liquid fraction for paraffin.

For solidification,

$$A_{mushy} = \frac{4\mu}{125\gamma^{0.3}} \times 10^{12} \tag{10}$$

For melting,

$$A_{mushy} = \frac{4\mu}{125\gamma} \times 10^{12} \tag{11}$$

Figure 8 shows the liquid fraction of the PCM for different values of A_{mushy} and compares it to simulation methods. The liquid fraction follows a similar trend across varying A_{mushy} values, with only slight differences toward the end of the solidification process. The solidification rate for $A_{mushy} = 10^8$ is faster than that for $A_{mushy} = 10^5$ in both the E-p and AHC methods, predicting a solidification time that aligns more closely with the new model. Furthermore, when A_{mushy} is variable, the liquid fraction profile remains the same as when A_{mushy} is constant at 10^8. Notably, the effects of different A_{mushy} values on the melting rate by the applied E-p method have been examined [40], and they reported that a significant variation in the mushy zone constant, from 10^5 to 10^8, led to a greater temperature difference.

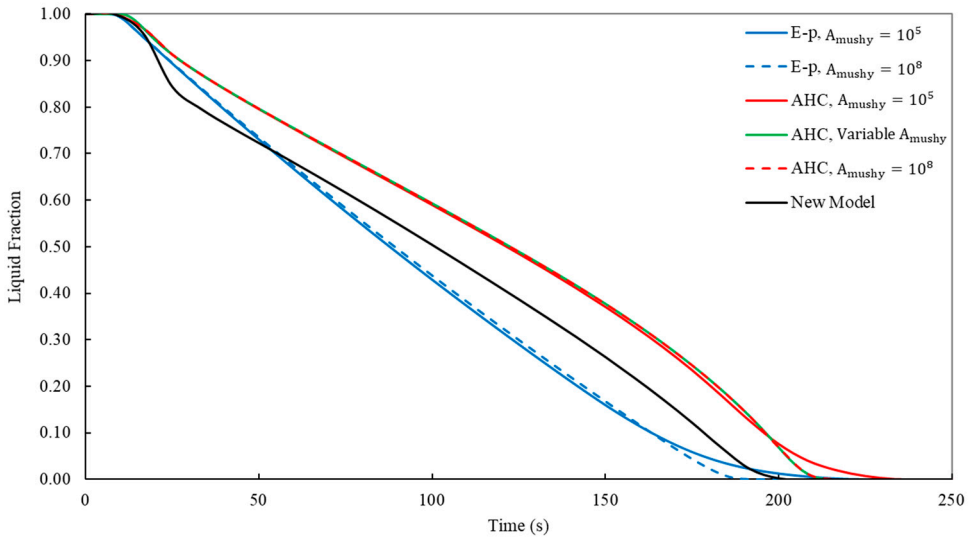

Figure 8. Consideration of the effect of variable A_{mushy} [51] on the liquid fraction.

To better understand the effect of A_{mushy} on the natural convection, it is worthwhile to consider the velocity contours for the PCM. These contours, shown in Figure 9, were generated via the mushy zone constants 10^5 and a variable mushy zone. At the initial stage of the solidification process, the liquid PCM near the cold wall loses heat, causing its temperature to decrease. This cooler liquid becomes denser and descends along the wall due to buoyancy forces. As the liquid moves away from the cold wall, it gains heat and its temperature rises, making it less dense and causing it to ascend to the top. This process results in a circulating flow driven by natural convection that initially develops within the liquid region. Figure 10 illustrates that the temperature difference decreases at a faster rate for the variable mushy zone parameter compared to the constant mushy zone parameter. As the temperature difference between the liquid and solid PCMs decreases, the velocity of

the liquid PCM along the solidification interface decreases and results in heat conduction being the dominant heat phenomena in solidification [52].

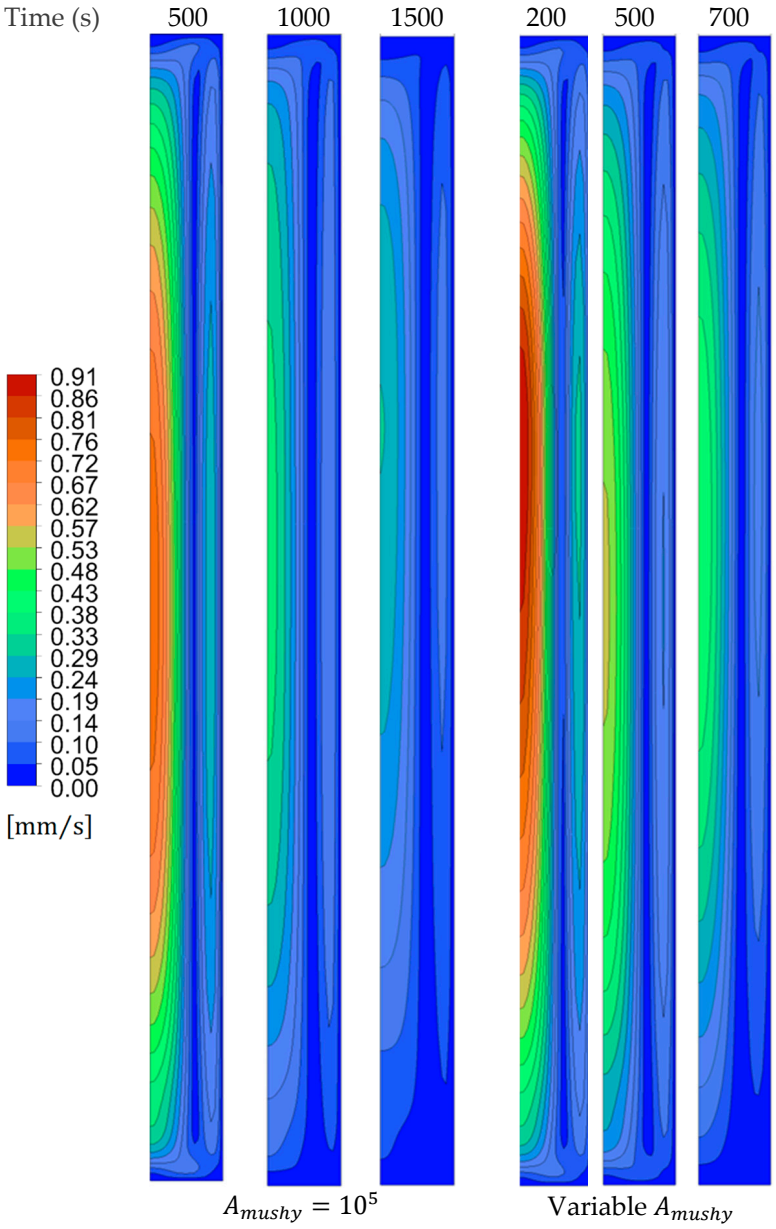

Figure 9. Comparison of the velocity contour lines inside the PCM during solidification.

Figure 10 compares the average velocity of natural convection for a baseline value of $A_{mushy} = 10^5$ and a variable A_{mushy}. For the variable mushy constant, the maximum velocity decreases sharply from approximately 0.23 mm/s at 1 min to 0 mm/s at 25 min, whereas for the constant mushy constant, it takes about 90 min to reach 0 mm/s. These temperature field evolutions indicate that the buoyancy-driven natural convection weakens over time, with heat transfer gradually becoming conduction-dominated. Notably, the variable mushy zone demonstrates higher values compared to $A_{mushy} = 10^5$, leading to stronger velocity damping as described by Equation (3).

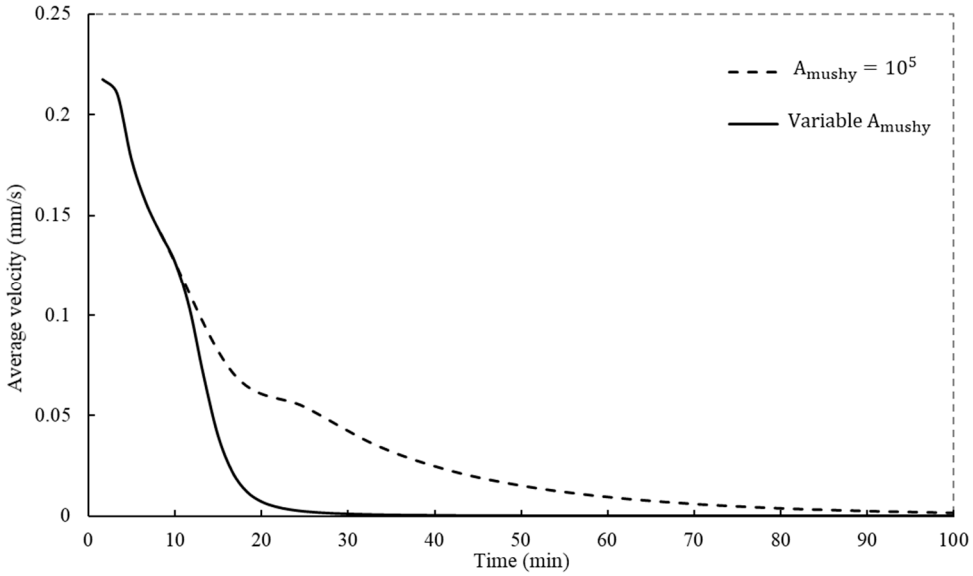

Figure 10. The impact of variable A_{mushy} [51] on the average velocity of natural convection.

4. Conclusions

The main goal of the current study was to examine the effect of the chosen numerical model of simulation and the mushy zone constant on the simulation of the solidification process inside a vertical cylinder for thermal energy storage applications. Three simulation models—enthalpy–porosity, AHC, and a new model—were applied to simulate solidification, and their results were compared. In the new numerical model, the specific heat capacity curve as a function of temperature, obtained from DSC, is directly introduced into ANSYS FLUENT. Additionally, a variable viscosity method accounts for the increased viscosity associated with the solid phase. Moreover, the effect of the mushy zone parameter on solidification was examined across the simulation models and the results were compared.

This study revealed that the proposed model shows excellent agreement with experimental data for cooling temperatures and provides a more accurate prediction than the other models, with an error margin of approximately 3.1%. The liquid fraction pattern for the new model and AHC is almost identical. In contrast, the E-p model displays a distinct pattern, with the solidification rate decreasing continuously until it reaches zero. Furthermore, the new model better satisfies the lumped system condition, showing less sensitivity to position in temperature variation than the other models. A_{mushy} is a critical parameter for accurately modeling phase change phenomena, as it gradually influences the prediction of solidification processes. Although the impact of A_{mushy} is more pronounced in the melting process, where heat transfer is primarily dominated by natural convection, its influence is generally less prominent in the solidification process, where conductive heat transfer is dominant. Increasing the mushy parameter value results in a reduction of the solidification time and similar results are observed for both a variable A_{mushy} and $A_{mushy} = 10^8$. A mushy zone constant of 10^8 has been proposed for the solidification process, which is in good agreement with the real results. Furthermore, this research demonstrates the importance of using accurate heat capacity and A_{mushy} values in simulations and highlights the potential errors that can result from simplifications or approximations. The criteria established in this study provide valuable guidance for accurately and effectively modeling the PCM behavior of paraffin in various applications, paving the way for future research.

Author Contributions: Conceptualization, methodology, formal analysis, data curation, supervision, validation, C.C.; project administration, funding acquisition, J.P.; formal analysis, software, investigation, writing—original draft preparation M.T.J.; resources, writing—review and editing, A.G.; funding acquisition, resources, writing—review and editing, I.A. All authors have read and agreed to the published version of the manuscript.

Funding: R&D project TED2021-131397B-100. Transición Ecológica en Areas Ru-rales-Ecological traN-Sition rUral aREas (ENSURE). MINISTERIO DE CIENCIA E INNOVACIÓN, MCIN/AEI/10.12039/501100011033/and European Union NextGenerationEU/PRTR.

Institutional Review Board Statement: Not applicable.

Informed Consent Statement: Not applicable.

Data Availability Statement: The data presented in this study are available on request from the corresponding author.

Conflicts of Interest: The authors declare no conflicts of interest.

References

1. Jamal-Abad, M.T.; Saedodin, S.; Aminy, M. Experimental Investigation on a Solar Parabolic Trough Collector for Absorber Tube Filled with Porous Media. *Renew. Energy* **2017**, *107*, 156–163. [CrossRef]
2. Jamal-Abad, M.T.; Saedodin, S.; Aminy, M. Heat Transfer in Concentrated Solar Air-Heaters Filled with a Porous Medium with Radiation Effects: A Perturbation Solution. *Renew. Energy* **2016**, *91*, 147–154. [CrossRef]
3. Zamzamian, A.; Keyanpour-Rad, M.; Kiani-Neyestani, M.; Jamal-Abad, M.T. An Experimental Study on the Effect of Cu-Synthesized/EG Nanofluid on the Efficiency of Flat-Plate Solar Collectors. *Renew. Energy* **2014**, *71*, 658–664. [CrossRef]
4. Jamal-Abad, M.T.; Saedodin, S.; Aminy, M. Variable Conductivity in Forced Convection for a Tube Filled with Porous Media: A Perturbation Solution. *Ain Shams Eng. J.* **2018**, *9*, 689–696. [CrossRef]
5. Imre, A.R.; Daniarta, S.; Błasiak, P.; Kolasiński, P. Design, Integration, and Control of Organic Rankine Cycles with Thermal Energy Storage and Two-Phase Expansion System Utilizing Intermittent and Fluctuating Heat Sources—A Review. *Energies* **2023**, *16*, 5948. [CrossRef]
6. Ehms, J.H.N.; Oliveski, R.D.C.; Rocha, L.A.O.; Biserni, C. Theoretical and Numerical Analysis on Phase Change Materials (PCM): A Case Study of the Solidification Process of Erythritol in Spheres. *Int. J. Heat Mass Transfer* **2018**, *119*, 523–532. [CrossRef]
7. Motahar, S.; Alemrajabi, A.A.; Khodabandeh, R. Experimental Study on Solidification Process of a Phase Change Material Containing TiO_2 Nanoparticles for Thermal Energy Storage. *Energy Convers. Manag.* **2017**, *138*, 162–170. [CrossRef]
8. Sefidan, A.M.; Taghilou, M.; Mohammadpour, M.; Sojoudi, A. Effects of Different Parameters on the Discharging of Double-Layer PCM through the Porous Channel. *Appl. Therm. Eng.* **2017**, *123*, 592–602. [CrossRef]
9. Tajik Jamal-Abad, M.; Cortés, C.; Pallarés Ranz, J.; Gil, A. Approximate Analytical Solution for Solidification of PCM in Cylindrical Geometry with Temperature-Dependent Thermal Conductivity—Perturbation Method. *J. Phys. Conf. Ser.* **2024**, *2766*, 012032. [CrossRef]
10. Peter, A.; Cornelia, O. Study on Solid–Liquid Interface Heat Transfer of PCM under Simultaneous Charging and Discharging (SCD) in Horizontal Cylinder Annulus. *Heat Mass Transfer* **2017**, *53*, 2223–2240. [CrossRef]
11. Sun, M.; Liu, T.; Wang, X.; Liu, T.; Li, M.; Chen, G.; Jiang, D. Roles of Thermal Energy Storage Technology for Carbon Neutrality. *Carb. Neutrality* **2023**, *2*, 12. [CrossRef]
12. Liu, A.; Xie, H.; Wu, Z.; Wang, Y. Advances and Outlook of TE-PCM System: A Review. *Carb. Neutrality* **2022**, *1*, 20. [CrossRef]
13. Liu, J.; Xiao, Y.; Chen, D.; Ye, C.; Nie, C. Melting and Solidification Characteristics of PCM in Oscillated Bundled-Tube Thermal Energy Storage System. *Energies* **2024**, *17*, 1973. [CrossRef]
14. Afaynou, I.; Faraji, H.; Choukairy, K.; Arıcı, M.; Khallaki, K. Heat Transfer Improvement of Phase Change Materials by Metal Foams and Nanoparticles for Efficient Electronic Thermal Management: A Comprehensive Study. *Int. J. Heat Mass Transfer* **2024**, *227*, 125534. [CrossRef]
15. Medjahed, B.; Arıcı, M.; Dardouri, S.; Chaib, S.; Goual, O.E.; Yüksel, A. Experimental Analysis of the Thermal Performance of Beeswax-Heat Exchanger as Latent Heat Thermal Energy Storage System. *J. Energy Storage* **2024**, *101*, 113898. [CrossRef]
16. Dardouri, S.; Medjahed, B.; Almoneef, M.M.; Mbarek, M. Thermal Behavior of Composite Material Based on Phase Change Material/Plaster as Thermal Energy Storage in Multilayer Wall: Experimental Study. *ACS Omega* **2024**, *9*, 24845–24852. [CrossRef] [PubMed]
17. Zhao, C.; Yan, J.; Tian, X.; Xue, X.; Zhao, Y. Progress in Thermal Energy Storage Technologies for Achieving Carbon Neutrality. *Carb. Neutrality* **2023**, *2*, 10. [CrossRef]
18. Jia, Y.; Jiang, Y.; Pan, Y.; Zou, X.; Zhang, Q.; Gao, X.; Zhang, J.; Yu, K.; Yang, Y.; Liu, Y. Recent advances in energy storage and applications of form-stable phase change materials with recyclable skeleton. *Carbon Neutralization* **2024**, *3*, 313–343. [CrossRef]
19. Kapilow, D.; Hsuan, Y.G.; Sun, Y.; McCarthy, M. Convective Melting and Freezing of Phase Change Materials Encapsulated within Small Diameter Polymer Tubes. *Exp. Therm. Fluid Sci.* **2018**, *92*, 259–269. [CrossRef]
20. Izgi, B.; Arslan, M. Numerical Analysis of Solidification of PCM in a Closed Vertical Cylinder for Thermal Energy Storage Applications. *Heat Mass Transfer* **2020**, *56*, 2909–2922. [CrossRef]
21. Allouche, Y.; Varga, S.; Bouden, C.; Oliveira, A. Validation of a CFD Model for the Simulation of Heat Transfer in a Tubes-in-Tank PCM Storage Unit. *Renew. Energy* **2016**, *89*, 371–379. [CrossRef]
22. Ye, W.; Zhu, D.; Wang, N. Fluid Flow and Heat Transfer in a Latent Thermal Energy Unit with Different Phase Change Material (PCM) Cavity Volume Fractions. *Appl. Therm. Eng.* **2012**, *42*, 49–57. [CrossRef]

23. Assis, E.; Katsman, L.; Ziskind, G.; Letan, R. Numerical and Experimental Study of Melting in a Spherical Shell. *Int. J. Heat Mass Transfer* **2007**, *50*, 1790–1804. [CrossRef]
24. Shmueli, H.; Ziskind, G.; Letan, R. Melting in a Vertical Cylindrical Tube: Numerical Investigation and Comparison with Experiments. *Int. J. Heat Mass Transfer* **2010**, *53*, 4082–4091. [CrossRef]
25. Wang, P.; Wang, X.; Huang, Y.; Li, C.; Peng, Z.; Ding, Y. Thermal Energy Charging Behavior of a Heat Exchange Device with a Zigzag Plate Configuration Containing Multiphase-Change-Materials (m-PCMs). *Appl. Energy* **2015**, *142*, 328–336. [CrossRef]
26. Silva, T.; Vicente, R.; Amaral, C.; Figueiredo, A. Thermal Performance of a Window Shutter Containing PCM: Numerical Validation and Experimental Analysis. *Appl. Energy* **2016**, *179*, 64–84. [CrossRef]
27. Hu, H.; Argyropoulos, S.A. Mathematical Modelling of Solidification and Melting: A Review. *Model. Simul. Mater. Sci. Eng.* **1996**, *4*, 371–396. [CrossRef]
28. Voller, V.R.; Brent, A.D.; Prakash, C. The Modelling of Heat, Mass and Solute Transport in Solidification Systems. *Int. J. Heat Mass Transfer* **1989**, *32*, 1719–1731. [CrossRef]
29. Ma, Z.; Zhang, Y. Solid Velocity Correction Schemes for a Temperature Transforming Model for Convection Phase Change. *Int. J. Numer. Methods Heat Fluid Flow* **2006**, *16*, 204–225. [CrossRef]
30. Ehms, J.H.N.; Oliveski, R.D.C.; Rocha, L.A.O.; Biserni, C.; Garai, M. Fixed Grid Numerical Models for Solidification and Melting of Phase Change Materials (PCMs). *Appl. Sci.* **2019**, *9*, 4334. [CrossRef]
31. Li, D.; Ren, Q.; Tong, Z.X.; He, Y.L. Lattice Boltzmann Models for Axisymmetric Solid–Liquid Phase Change. *Int. J. Heat Mass Transfer* **2017**, *112*, 795–804. [CrossRef]
32. Kabbara, M.; Kheirabadi, A.C.; Groulx, D. Numerical Modeling of Natural Convection Driven Melting for an Inclined/Finned Rectangular Enclosure. In Proceedings of the ASME 2016 Heat Transfer Summer Conference, HT 2016, Collocated with the ASME 2016 Fluids Engineering Division Summer Meeting and the ASME 2016 14th International Conference on Nanochannels, Microchannels, and Minichannels, Washington, DC, USA, 10–14 July 2016; Volume 2. [CrossRef]
33. Kheirabadi, A.C.; Groulx, D. The Effect of the Mushy-Zone Constant on Simulated Phase Change Heat Transfer. In Proceedings of the CHT-15 ICHMT International Symposium on Advances in Computational Heat Transfer, Piscataway, NJ, USA, 25–29 May 2015; p. 2. [CrossRef]
34. Abdi, A.; Martin, V.; Chiu, J.N.W. Numerical Investigation of Melting in a Cavity with Vertically Oriented Fins. *Appl. Energy* **2019**, *235*, 1027–1040. [CrossRef]
35. Hong, Y.; Ye, W.B.; Du, J.; Huang, S.M. Solid–Liquid Phase-Change Thermal Storage and Release Behaviors in a Rectangular Cavity under the Impacts of Mushy Region and Low Gravity. *Int. J. Heat Mass Transfer* **2019**, *130*, 1120–1132. [CrossRef]
36. Fadl, M.; Eames, P.C. Numerical Investigation of the Influence of Mushy Zone Parameter Amush on Heat Transfer Characteristics in Vertically and Horizontally Oriented Thermal Energy Storage Systems. *Appl. Therm. Eng.* **2019**, *151*, 90–99. [CrossRef]
37. Vogel, J.; Felbinger, J.; Johnson, M. Natural Convection in High-Temperature Flat Plate Latent Heat Thermal Energy Storage Systems. *Appl. Energy* **2016**, *184*, 184–196. [CrossRef]
38. Chen, C.Q.; Diao, Y.H.; Zhao, Y.H.; Wang, Z.Y.; Liang, L.; Chi, Y.Y. Experimental and Numerical Investigations of a Lauric Acid-Multichannel Flat Tube Latent Thermal Storage Unit. *Int. J. Energy Res.* **2018**, *42*, 4070–4084. [CrossRef]
39. Sciacovelli, A.; Colella, F.; Verda, V. Melting of PCM in a Thermal Energy Storage Unit: Numerical Investigation and Effect of Nanoparticle Enhancement. *Int. J. Energy Res.* **2013**, *37*, 1610–1623. [CrossRef]
40. Martínez, M.A.; Carmona, M.; Cortés, C.; Arauzo, I. Experimentally Based Testing of the Enthalpy-Porosity Method for the Numerical Simulation of Phase Change of Paraffin-Type PCMs. *J. Energy Storage* **2023**, *69*, 107876. [CrossRef]
41. Fluent, A. *R2 User's Manual*; ANSYS Inc.: Canonsburg, PA, USA, 2020.
42. Jamal-Abad, M.T.; Martínez, A.; Carmona, M.; Cortes, C. Numerical Analysis of Solidification of Paraffin-Type PCMs by Using Customary Fixed Grid Methods. *Manuscript submitted for publication*.
43. Tajik Jamal-Abad, M.; Cortes, C.; Martínez, A.; Carmona, M. Numerical Investigation of the Effect of the Mushy Zone Parameter and the Thermal Properties of Paraffin-Based PCMs on Solidification Modeling under T-History Conditions. *Authorea* **2024**. [CrossRef]
44. Voller, V.R.; Cross, M.; Markatos, N.C. An Enthalpy Method for Convection/Diffusion Phase Change. *Int. J. Numer. Methods Eng.* **1987**, *24*, 271–284. [CrossRef]
45. Barz, T.; Buruzs, A.; Sommer, A. Major and minor hysteresis loops in the enthalpy-temperature and phase fraction-temperature diagrams of solid/liquid phase change materials. *Int. J. Eng. Sci.* **2023**, *191*, 103913. [CrossRef]
46. Barz, T.; Bres, A.; Emhofer, J. slPCMlib: A Modelica Library for the Prediction of Effective Thermal Material Properties of Solid/Liquid Phase Change Materials (PCM). In Proceedings of the Asian Modelica Conference 2022, Tokyo, Japan, 24–25 November 2022; pp. 63–74.
47. Buruzs, A.; Giordano, F.; Schieder, M.; Reichl, C.; Goderis, M.; Beyne, W.; De Paepe, M.; Barz, T. CFD Simulation of Solid/Liquid Phase Change in Commercial PCMs Using the slPCMlib Library. *J. Phys. Conf. Ser.* **2024**, *2766*, 012223. [CrossRef]
48. Salcudean, M.; Abdullah, Z. On the Numerical Modelling of Heat Transfer during Solidification Processes. *Int. J. Numer. Methods Eng.* **1988**, *25*, 445–473. [CrossRef]
49. Gartling, D.K. *Computer Methods in Fluids*; Morgan, K., Taylor, C., Brebbia, C.A., Eds.; Pentech: London, UK, 1980; pp. 219–230.
50. Yang, B.; Bai, F.; Wang, Y.; Wang, Z. How Mushy Zone Evolves and Affects the Thermal Behaviors in Latent Heat Storage and Recovery: A Numerical Study. *Int. J. Energy Res.* **2020**, *44*, 4279–4297. [CrossRef]

51. Yang, B.; Raza, A.; Bai, F.; Zhang, T.; Wang, Z. Microstructural Evolution within Mushy Zone during Paraffin's Melting and Solidification. *Int. J. Heat Mass Transfer* **2019**, *141*, 769–778. [CrossRef]
52. Ezzat, Y.; Sakr, R.Y.; Abdel-Rehim, A.A. Numerical Investigation of the Effect of Thermal Expansion Coefficient and Mushy Zone Constant on Modeling of the Phase Change Process to Provide Reliable Selection Criteria of Modeling Parameters. *J. Energy Storage* **2023**, *72*, 108771. [CrossRef]

Disclaimer/Publisher's Note: The statements, opinions and data contained in all publications are solely those of the individual author(s) and contributor(s) and not of MDPI and/or the editor(s). MDPI and/or the editor(s) disclaim responsibility for any injury to people or property resulting from any ideas, methods, instructions or products referred to in the content.